

Coherent Topological Transport on the Surface of Bi_2Se_3

Dohun Kim¹, Paul Syers¹, Nicholas P. Butch², Johnpierre Paglione¹, and Michael S. Fuhrer^{1*}

1. Center for Nanophysics and Advanced Materials, Department of Physics, University of Maryland, College Park, MD 20742-4111, USA

2. Condensed Matter and Materials Division, Lawrence Livermore National Laboratory, Livermore, CA 94550, U.S.A.

The two-dimensional (2D) surface state of the three-dimensional strong topological insulator (STI) is fundamentally distinct from other 2D electron systems¹ in that the Fermi arc encircles an odd number of Dirac points²⁻⁸. The TI surface is in the symplectic universality class and uniquely among 2D systems remains metallic and cannot be localized by (time-reversal symmetric) disorder⁹. However, in finite-size samples inter-surface coupling can destroy the topological protection¹⁰⁻¹². The question arises: At what size can a thin TI sample be treated as having decoupled topological surface states? We show that weak anti-localization¹³⁻²¹ (WAL) is extraordinarily sensitive to sub-meV coupling between top and bottom topological surfaces, and the surfaces of a TI film may be coherently coupled even for thicknesses as large as 12 nm. For thicker films we observe the signature of a true 2D topological metal: perfect weak anti-localization in quantitative agreement with two decoupled surfaces in the symplectic symmetry class.

Weak localization (WL) and weak anti-localization (WAL) describe corrections to the classical electrical conductivity of two-dimensional electron gases due to coherent interference of time-reversed paths. The TI surface state is in the symplectic symmetry class and expected to exhibit perfect WAL described by Higami, Larkin and Nagaoka¹³:

$$\Delta\sigma(H) = \alpha \frac{e^2}{\pi h} \left[\ln \frac{H_0}{H} - \psi \left(\frac{1}{2} + \frac{H_0}{H} \right) \right] \quad (1)$$

where $H_0 = \hbar/4D\tau_\phi$ is a characteristic field related to the phase coherence time τ_ϕ and diffusion constant D , ψ is the digamma function, and α is the overall amplitude whose expected value for a single 2D channel is 1/2. However, WAL is sensitive to the competition between the phase coherence time τ_ϕ and other time scales²²; in TI thin films, carriers may scatter into additional conducting channels (from top to bottom surface, or into the conducting bulk), modifying the WAL behavior. In contrast to previous studies of WAL in TI thin films¹³⁻²¹ where strong surface to bulk scattering dominates inter-channel coupling, we measure WAL in gate-tuned, bulk insulating Bi₂Se₃ thin films where we expect negligible surface-bulk scattering. We find that the WAL behavior is governed by the ratio of τ_ϕ to the inter-surface tunneling time $\tau_t = \hbar/2\Delta$ where \hbar is Planck's constant and Δ is the hybridization gap induced by inter-surface tunneling^{10,12}. For thick films, $\tau_\phi/\tau_t < 1$ and we observe WAL according to Eqn. [1] with $\alpha = 1/2 + 1/2 = 1$ corresponding to two decoupled TI surfaces each with $\alpha = 1/2$. A thickness and doping-dependent crossover is observed when $\tau_\phi/\tau_t > 1$ to a regime where $\alpha = 1/2$, indicating the coherent coupling of two TI surfaces. For even thinner samples, Δ becomes comparable to the disorder strength and the Berry's phase is completely randomized at low carrier density causing the suppression of WAL and WL, reflecting the loss of topological protection for strongly coupled surfaces.

We study mechanically exfoliated Bi₂Se₃ single crystals²³ ranging in thickness from 5 to 17 quintuple layers (QL). Figure 1a shows a representative device (thickness 12 QL), where height profiles across the width direction of the 17, 12, 7, and 5 QL devices are shown in figure 1b. In order to achieve the topological transport regime we employed molecular charge transfer *p*-type doping by thermal evaporation of 2,3,5,6-tetrafluoro-7,7,8,8-tetracyanoquinodimethane, described previously²⁴ (see also Methods and Supplementary Information S1).

Figure 1c and d show the longitudinal resistivity ρ_{xx} and Hall carrier density $n_H = 1/(eR_H)$ (where R_H is the Hall coefficient, and e is the elementary charge) of the devices at a temperature of 2K as a function of back gate voltage V_g . We measure n_H in the range of 2-7 x 10¹² cm⁻² at zero gate voltage. The carrier density in the topological surface state at the bulk conduction band edge is approximately 1.0 x 10¹³ cm⁻² hence the devices are in the TI regime before application of a back gate voltage. Ambipolar electric field effects are indicated by the sharp peak of $\rho_{xx}(V_g)$ and the sign change in n_H at the charge neutrality points ($V_{g,0}$, figure. 1c dashed lines). The dependence of $\rho_{xx}(V_{g,0})$ on temperature T in all of our devices, including 5 QL, shows metallic behavior (See Supplementary Information S2) which is likely due to conduction through inhomogeneity-driven electron-hole puddles^{24,25}. However the thinnest (5 QL) device shows an anomalously large maximum $\rho_{xx}(V_{g,0})$ of about 23 k Ω which cannot be understood within the self-consistent theory for a Dirac band in the presence of charge disorder^{24,26,27}, suggesting that the inter-surface hybridization gap Δ becomes important in determining the resistivity in this regime¹⁰. We note that true insulating behavior (divergent ρ_{xx} as $T \rightarrow 0$) is not observed for the 5 QL sample, but was previously observed for 3QL Bi₂Se₃ [11]. More work is needed to understand the ρ_{xx} maximum in the 5 QL sample (See Supplementary Information S2 for further discussion).

We now turn to discuss gate-tuned WAL behavior in the TI regime. Figure 2 shows the magneto-conductivity $\Delta\sigma(H)$ for all four devices. Curves are taken at similar carrier density $n = C_g(V_g - V_{g,0})/e$ (where gate capacitance $C_g \approx 11 \text{ nFcm}^{-2}$) ranging from $\approx 7 \times 10^{12} \text{ cm}^{-2}$ (n -type) to $-2 \times 10^{12} \text{ cm}^{-2}$ (p -type) except for the 17 QL device where only n -type carrier density (7 and $2 \times 10^{12} \text{ cm}^{-2}$) could be observed due to relatively high initial doping. The data for the entire range of n and thickness can be fitted (dashed curves in Fig. 2) well with Eqn. (1). The validity of Eqn. (1) in the multichannel limit has been addressed in a number of previous studies^{14, 18, 19, 28}, finding that Eqn. [1], in particular the logarithmic correction term, provides a robust physical description of WAL behavior even in the multichannel limit irrespective of the Drude conductivity of each channel^{19, 28}. Therefore $\alpha = m/2$ probes the number of channels m .

Figure 3 shows the variation of α obtained from the fit to Eqn. (1) as a function of n for 17 (black), 12 (red), 7 (green), and 5 (blue) QL devices measured at 2 K. In all devices α is close to $1/2$ at high $n \approx 8 \times 10^{12} \text{ cm}^{-2}$, which we interpret as WAL in a single strongly coupled coherent channel^{14-16, 18, 19}. However, the behavior of α upon gate tuning shows very different behaviors depending on the thickness of the devices. The thickest device (17 QL) shows WAL consistent with two decoupled top and bottom topological surfaces ($\alpha \approx 1$) starting at moderate $n \approx 6 \times 10^{12} \text{ cm}^{-2}$, maintained down to the minimum accessible n . Similar variation of α ranging from 0.7 to 1 was observed in Ref. [19] with the application of top gate, and interpreted there as the decoupling of top surface and bulk (plus bottom) channels due to formation of band-bending induced depletion layer. We do not rule out the possible contribution of bulk-surface scattering in 17 QL at high n . However, we note that this effect alone cannot explain the general behavior of α for low n and thinner devices. Notably, we identify two crossovers in the 12 QL device: we observe sharp transition of α from $\approx 1/2$ to ≈ 1 near $n \approx 1 \times 10^{12} \text{ cm}^{-2}$ (n -type), and back to $1/2$ at

$n \approx -1 \times 10^{12} \text{cm}^{-2}$ (*p*-type). $\Delta\sigma(H)$ in our devices include a moderate contribution from (universal) conductance fluctuations (Fig. 2), as commonly observed in micro-fabricated Bi_2Se_3 devices^{15,20}. However we repeated similar WAL measurements at 2 K for the 12 QL device on five different thermal runs, where the conductance fluctuation contribution is randomized, and find that the crossovers are reproducible within the experimental uncertainty (Fig. 3, error bars). This transition is absent in the 7 QL device where WAL in the entire range of n indicates a strongly coupled single channel ($\alpha \approx 1/2$). Finally, at an even smaller thickness (5QL), we observe strong suppression of WAL for $-1 \times 10^{12} \text{cm}^{-2} < n < 1 \times 10^{12} \text{cm}^{-2}$, (inset of Fig. 3, see also Fig. 2d).

We now examine the coherence time τ_ϕ and compare to the estimated interlayer tunnel time τ_t . We estimate $\tau_\phi = \hbar/4eDH_0$ from the fits to Eqn. [1] and using $D = \tau v_f^2/2$ where Fermi velocity $v_f \approx 3 \times 10^7 \text{cm/s}$ for Bi_2Se_3 [29], and the momentum relaxation time τ is calculated from the measured $\sigma(n)$. τ_t represents the characteristic time of transition (half the period Rabi oscillations) between localized states in two quantum wells with energy splitting Δ , thus $\tau_t = \hbar/2\Delta$. We estimate Δ in Bi_2Se_3 by fitting the existing experimental data¹⁰ to an exponentially decaying function, $\Delta(t) = [992 \text{ meV}]e^{-0.67[t \text{ (nm)}]}$, and obtain Δ of 34.8, 9.1, 0.3, and 0.01 meV for 5, 7, 12, and 17 QL, respectively. (Theoretical calculations of finite size effects in Bi_2Se_3 predict systematically smaller Δ at a given thickness and also suggest that Δ shows oscillatory decaying behavior¹², which do not seem to be observed in the previous work¹⁰ or this work.)

Figure 4 shows the estimated τ_ϕ and τ_t as functions of n for the different thickness samples. Upon gate tuning, τ_ϕ changes by an order of magnitude ranging from ≈ 4 to $\approx 50 \text{ ps}$, and shows a sharp dip near $n = 0$. For the 17 QL device, $\tau_\phi/\tau_t \ll 1$ in the entire range of n . In this limit electrons on either surface lose coherence before scattering to the other, thus each surface acts as

an independent coherent transport channel and $\alpha \approx 1$. In contrast a crossover occurs from $\tau_\phi/\tau_t \gg 1$ at high unipolar n - and p -type carrier densities to $\tau_\phi/\tau_t < 1$ near $n = 0$ in the 12 QL device, which is consistent with the observed crossover from $\alpha = 1/2$ to $\alpha = 1$ (Fig. 3). In the thinner device (7 QL), the condition $\tau_\phi/\tau_t \gg 1$ is satisfied, and the two surfaces are strongly coupled ($\alpha \approx 1/2$) for the entire range of n . In contrast to semi-classical Boltzmann transport in Bi_2Se_3 TI films, where the signature of finite size effect appear only in the ultrathin limit ($\leq 3\text{QL}$)¹¹, phase coherent transport offers an exquisitely sensitive probe of the hybridization of top and bottom transport channels, detecting a gap Δ as small as 0.3 meV in the 12 QL TI film¹⁰.

The behavior described above is in general consistent in the 5 QL device except near the Dirac point, where WAL is strongly suppressed. The suppression of WAL can be understood in terms of the expected change of Berry phase $\theta_B = \pi(1 - \Delta/2E_f)$ in TIs³⁰ as a function of Δ and the Fermi energy E_f ; θ_B is reduced from π when hybridization induced gap opens. Assuming a gapped Dirac dispersion $E_f = \sqrt{(\hbar v_f k_f)^2 + (\Delta/2)^2}$, we estimate $E_f \leq 52$ meV and $\theta_B \leq 0.67\pi$ at $|n| \leq 1 \times 10^{12} \text{ cm}^{-2}$. This range of n is comparable to the electron-hole puddle density $n^* \approx 0.5 \times 10^{12} \text{ cm}^{-2}$ per surface (Fig. 1d) hence transport occurs through a landscape of electron and hole puddles with θ_B spanning the entire range $0 \leq \theta_B \leq \pi$. It appears that in this regime of highly inhomogeneous Berry phase that both WAL and WL (expected as $\theta_B \rightarrow 0$) are suppressed. We note that similar suppression of WAL was recently observed in thin epitaxial Bi_2Se_3 of varying thickness (and Δ) but fixed E_f [21], and a competition between WAL and WL was observed in gated 4 QL epitaxial $(\text{Bi}_{0.57}\text{Sb}_{0.43})_2\text{Te}_3$ [31]. Our observation of the WAL suppression by tuning both E_f and Δ (thickness) allows us to identify the ratio of τ_ϕ/τ_t as the driver for the crossover

between coupled and decoupled surfaces, and the ratio of Δ to disorder strength as the driver for the crossover to the regime of suppressed WAL/WL.

Methods

Low-doped (carrier density $\sim 10^{17} \text{ cm}^{-3}$) bulk Bi_2Se_3 single crystals with bulk resistivity exceeding $2 \text{ m}\Omega \text{ cm}$ at 300 K were grown by melting high purity bismuth (6N) and selenium (5N) in sealed quartz ampoules²³. Crystals were exfoliated with Scotch tape and deposited on doped Si covered with 300 nm SiO_2 . Thin Bi_2Se_3 crystals with thickness ranging from 5 to 17 nm were identified by combined use of optical and atomic force microscopy (AFM). From the AFM height profile of Bi_2Se_3 thin flakes, atomically flat surfaces with height variation less than 1 QL were chosen as channel area. Electron beam lithography, thermal evaporation and liftoff techniques were used to make electrical contact (Cr/Au: $5/70 \text{ nm}$). For accurate determination of the geometric factor, thin films were patterned into Hall bar geometry (see Fig. 1a) with typical aspect ratio (L/W) of about 2 and shortest length exceeding $2 \mu\text{m}$ using Ar plasma at a pressure of $\sim 6.7 \text{ Pa}$ ($5 \times 10^{-2} \text{ Torr}$). Molecular charge transfer doping was done by thermal evaporation of $\sim 10 \text{ nm}$ of 2,3,5,6-tetrafluoro-7,7,8,8-tetracyanoquinodimethane organic molecules (Aldrich) on top of the fabricated samples²⁴.

Transport measurements were performed using standard four-probe ac methods with low frequency ($< 17 \text{ Hz}$) excitation currents (rms amplitude 100 nA) using Stanford Research Systems SR830 Lock in amplifiers and a commercial cryostat equipped with 9 T superconducting magnet. For the 12 QL device, five different WAL measurements as a function of gate voltage at 2 K were conducted, where the sample was warmed up to 300 K and exposed to air for a few hours between thermal runs.

Acknowledgements

This work was supported by NSF grant number DMR-1105224. Preparation of Bi_2Se_3 was supported by NSF MRSEC (DMR-0520471) and DARPA-MTO award (N66001-09-c-2067). NPB was partially supported by the Center for Nanophysics and Advanced Materials. D. Kim acknowledges useful conversations with Sergey S. Pershoguba.

Author Contributions

D.K. fabricated devices, performed the electrical measurements, and analyzed the data with M.S.F. P.S., N.P.B, and J.P. prepared single crystal Bi_2Se_3 starting material. D.K. and M.S.F. wrote the manuscript with contributions from all authors.

Additional Information

The authors declare no competing financial interests. Supplementary information accompanies this paper. Correspondence and requests for materials should be addressed to Michael S. Fuhrer (mfuhrer@umd.edu).

References

1. Novoselov, K. S. *et al.* Two-dimensional gas of massless Dirac fermions in graphene. *Nature* **438**, 197-200 (2005).
2. Qi, X.L. & Zhang, S.-C. Topological insulators and superconductors. *Rev. Mod. Phys.* **83**, 1057-1110 (2011).
3. Hasan, M. Z., Kane, C. L. Colloquium: Topological insulators. *Rev. Mod. Phys.* **82**, 3045-3067 (2010)
4. Moore, J. Topological insulators: The next generation. *Nature Phys.* **5**, 378-380 (2009).
5. Zhang, H. J. *et al.* Topological insulators in Bi_2Se_3 , Bi_2Te_3 and Sb_2Te_3 with a single Dirac cone on the surface. *Nature Phys.* **5**, 438-442 (2009).
6. Hsieh, D. *et al.* A tunable topological insulator in the spin helical Dirac transport regime. *Nature* **460**, 1101-1105 (2009).

7. Chen, Y. L. *et al.* Experimental realization of a three-dimensional topological Insulator Bi_2Te_3 . *Science* **325**, 178-181 (2009).
8. Xia, Y. *et al.* Observation of a large-gap topological-insulator class with a single Dirac cone on the surface. *Nature Phys.* **5**, 398-402 (2009).
9. Fu, L., Kane, C. L. & Mele, E. J. Topological insulators in three dimensions. *Phys. Rev. Lett.* **98**, 106803 (2007).
10. Zhang, Y. *et al.* Crossover of the three-dimensional topological insulator Bi_2Se_3 to the two-dimensional limit *Nature Phys.* **6**, 584-588 (2010).
11. Cho, S., Butch, N. P., Paglione, J., & Fuhrer, M. S. Insulating behavior in ultrathin bismuth selenide field effect transistors. *Nano Lett.* **11**, 1925-1927 (2011).
12. Linder, J., Yokoyama, T., & Sudbø, A. Anomalous finite size effects on surface states in the topological insulator Bi_2Se_3 . *Phys. Rev. B* **80**, 205401 (2009).
13. Hikami, S., Larkin, A. I., & Nagaoka, Y. Spin-Orbit Interaction and Magnetoresistance in the Two Dimensional Random System. *Prog. Theor. Phys.* **63**, 707-710 (1980).
14. Chen, J. *et al.* Gate-Voltage Control of Chemical Potential and Weak Antilocalization in Bi_2Se_3 . *Phys. Rev. Lett.* **105**, 176602 (2010).
15. Checkelsky, J. G. Hor, Y. S., Cava R. J. & Ong N. P. Surface state conduction observed in voltage-tuned crystals of the topological insulator Bi_2Se_3 . *Phys. Rev. Lett.* **106**, 196801 (2010).
16. Kim, Y. S. *et al.* Thickness-dependent bulk properties and weak antilocalization effect in topological insulator Bi_2Se_3 . *Phys. Rev. B* **84**, 073109 (2011).
17. He, H.-T. *et al.* Impurity effect on weak antilocalization in the topological insulator Bi_2Te_3 . *Phys. Rev. Lett.* **106**(16), 166805 (2011).
18. Chen, J. *et al.* Tunable surface conductivity in Bi_2Se_3 revealed in diffusive electron transport. *Phys. Rev. B* **83**, 241304 (2011).
19. Steinberg, H., Laloe, J. B., Fatemi, V., Moodera, J. S., & Jarillo-Herrero, P. Electrically tunable surface-to-bulk coherent coupling in topological insulator thin films. *Phys. Rev. B* **84**, 233101 (2011).
20. Matsuo, S. *et al.* Weak antilocalization and conductance fluctuation in a submicrometer-sized wire of epitaxial Bi_2Se_3 . *Phys. Rev. B* **85**, 075440 (2012).
21. Taskin, A. A., Sasaki, S., Segawa, K., & Ando, Y. Manifestation of topological protection in transport properties of epitaxial Bi_2Se_3 thin films *Phys. Rev. Lett.* **109**, 066803 (2012)
22. Beenakker, C. W. J. , & Houten, H. V. Quantum Transport in Semiconductor Nanostructures *Solid State Physics* **44**, 1-228 (1991)
23. Butch, N. P. *et al.* Strong surface scattering in ultrahigh-mobility Bi_2Se_3 topological insulator crystals. *Phys. Rev. B* **81**, 241301 (2010).
24. Kim, D. *et al.* Surface conduction of topological Dirac electrons in bulk insulating Bi_2Se_3 *Nature Phys.* **8**, 460-464 (2012)
25. Beidenkopf, H. *et al.* Spatial fluctuations of helical Dirac fermions on the surface of topological insulators. *Nature Phys.* **7**, 939-943 (2011)
26. Adam, S., Hwang, E. H., Galitski, V. M. & Das Sarma, S. A self-consistent theory for graphene transport. *P. Natl. Acad. Sci. USA* **104**, 18392-18397 (2007).
27. Adam, S., Hwang, E. H. & Das Sarma, S. Two-dimensional transport and screening in topological insulator surface states. *Phys. Rev. B* **85**, 235413 (2012)
28. Garate, I., & Glazman, L. Weak localization and antilocalization in topological insulator thin films with coherent bulk-surface coupling *Phys. Rev. B* **86**, 035422 (2012)
29. Zhu, Z. H. *et al.*, Rashba spin-splitting control at the surface of the topological insulator Bi_2Se_3 *Phys. Rev. Lett.* **107** 186405 (2011).
30. Lu, H. Z., Shi, J., & Shen, S.Q. Competition between weak localization and antilocalization in topological surface states *Phys. Rev. Lett.* **107**, 076801 (2011)
31. Lang, M. *et al.* Competing weak localization and weak antilocalization in ultrathin topological insulators. *Nano. Lett. Article ASAP* (2012)

Figure captions

Figure 1 Characterization of Bi₂Se₃ Hall bar devices. **a**, AFM image of 12 QL Bi₂Se₃ Hall bar device. **b**, Height profiles along width directions of the devices used in this study. **c**, Longitudinal resistivity ρ_{xx} and **d**, sheet carrier density n_H determined from Hall measurement as a function of back gate voltage at the temperature of 2 K for 17 (black), 12 (red), 7 (green), and 5 (blue) QL devices. The dashed lines show charge neutrality points.

Figure 2 Weak anti-localization in the topological insulator regime. Magneto-conductivity $\Delta\sigma$ as a function of perpendicular magnetic field H in **a**, 17, **b**, 12, **c**, 7, and **d**, 5QL devices measured at 2 K at gate-induced carrier densities indicated in the legends. Dashed curves show least-square fits to Eqn. [1]. Zeros of all curves are offset by $0.7 e^2/h$ for clarity.

Figure 3 Coupled / decoupled coherent transport in Bi₂Se₃ surface states. Variation of the amplitude of weak anti-localization α as a function of 2D carrier density n for 17 (black square), 12 (red circle), 7 (green triangle), and 5 QL (blue triangle) thick devices measured at 2K. For the 12 QL device, the error bars show standard deviations determined from WAL measurements taken at five different thermal runs. The inset shows detailed behavior of suppression of WAL for 5 QL at small n .

Figure 4 Phase coherence time (τ_ϕ) vs. interlayer tunneling time (τ_t). Comparison of phase coherence time τ_ϕ determined from fit to Eqn. [1] and transport scattering time to interlayer tunneling time τ_t estimated from surface hybridization induced energy gap Δ as a function of 2D

carrier density n . Symbols are experimentally measured τ_ϕ for 17 (black square), 12 (red circle), 7 (green triangle), and 5 QL (blue triangle) devices. The dashed lines with corresponding colors show estimated inter-surface tunneling time τ_t .

Figure 1.

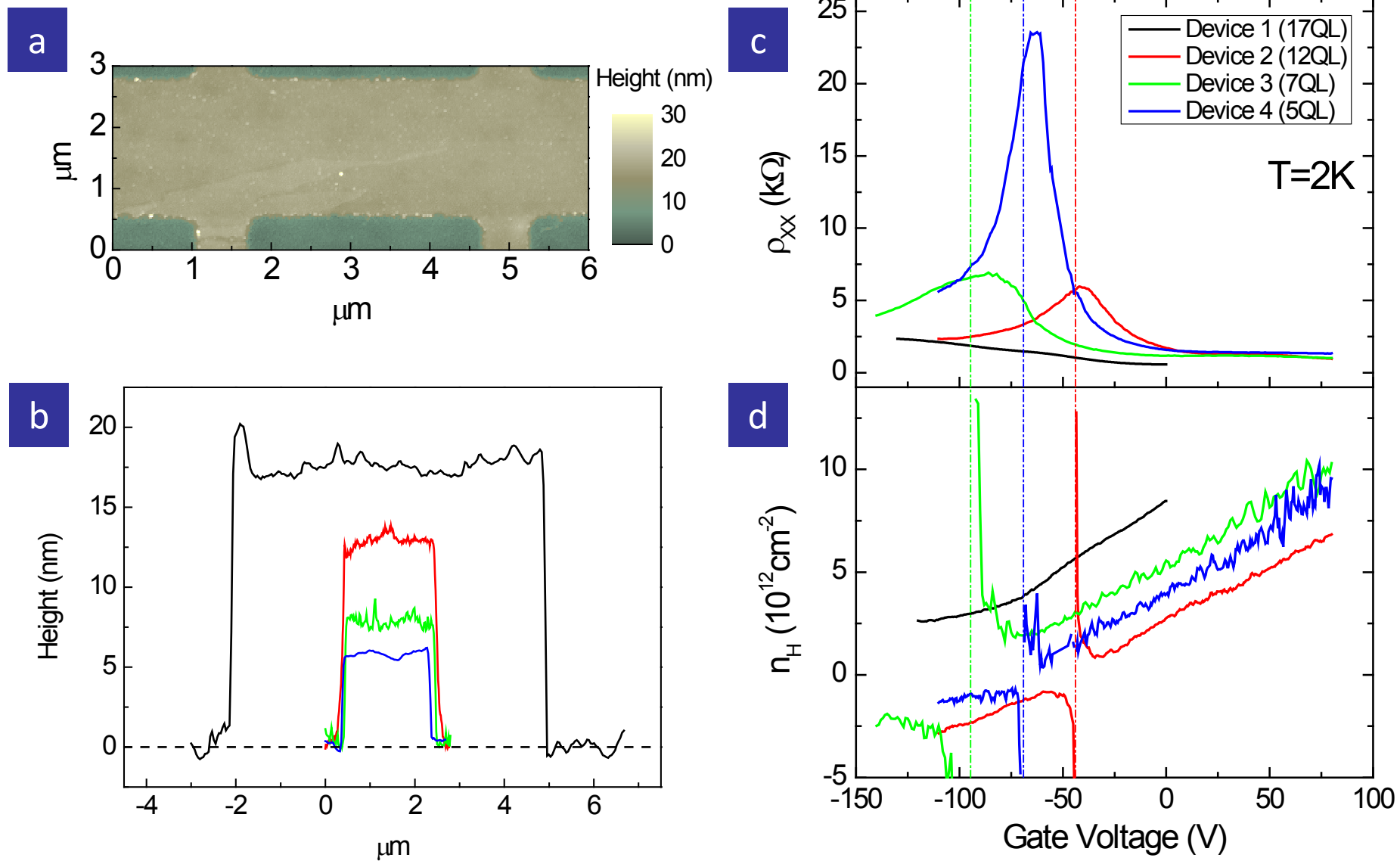


Figure 2.

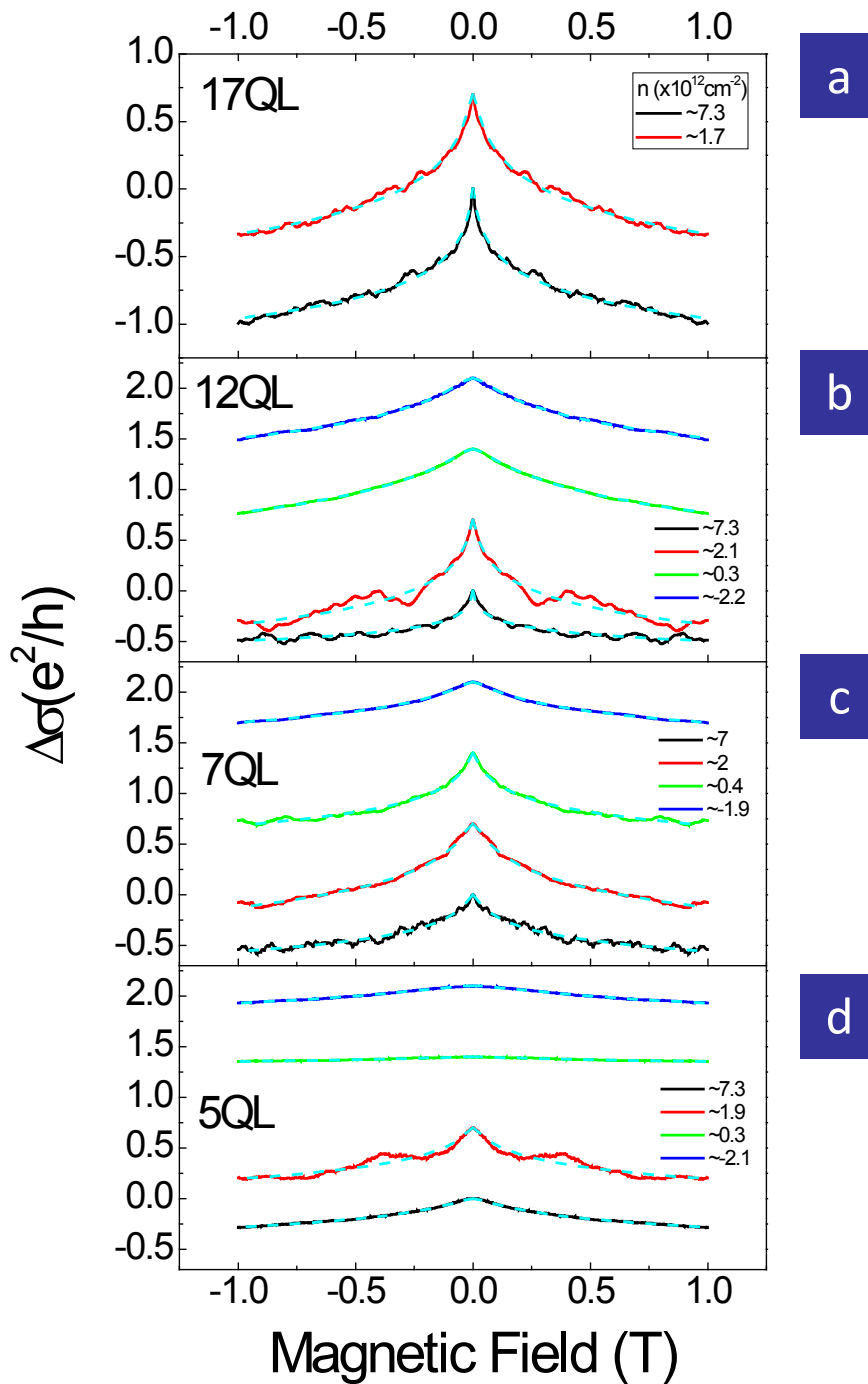
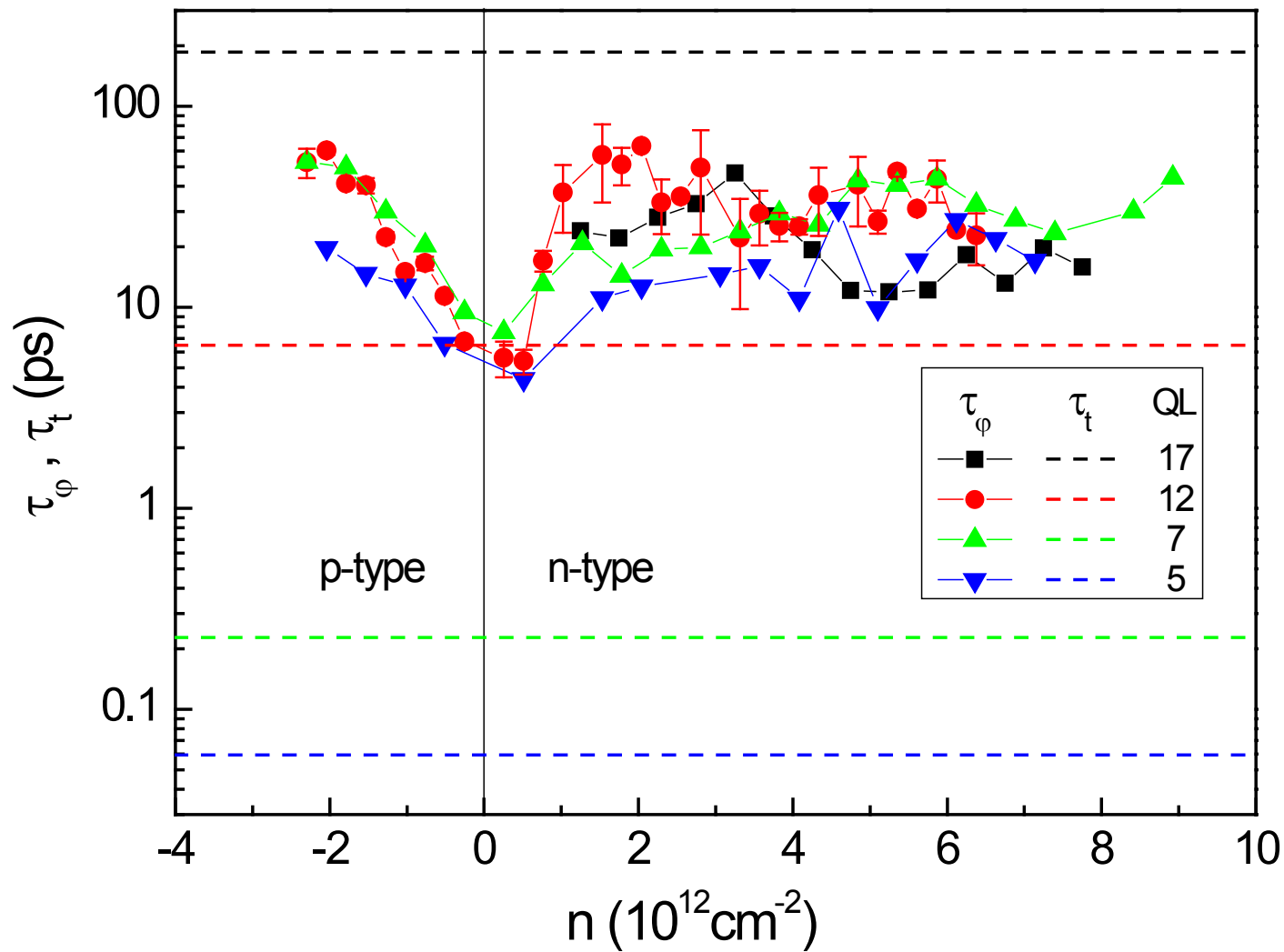


Figure 4.



Coherent Topological Transport on the Surface of Bi_2Se_3

Dohun Kim¹, Paul Syers¹, Nicholas P. Butch², Johnpierre Paglione¹, and Michael S. Fuhrer^{1*}

1. Center for Nanophysics and Advanced Materials, Department of Physics, University of Maryland, College Park, MD 20742-4111, USA

2. Condensed Matter and Materials Division, Lawrence Livermore National Laboratory, Livermore, CA 94550, U.S.A.

Supplementary Information

1. Charge transfer *p*-type doping with F4TCNQ : statistics and stability

Reducing unintentional doping in TIs is of central importance in realizing surface-dominant conduction. Here we adopt surface charge-transfer doping which provides simple and effective method for *p*-type doping TI thin films^{5,11}. The doping agent we consider is 2,3,5,6-tetrafluoro-7,7,8,8-tetracyanoquinodimethane (F4TCNQ). It has high electron affinity (≈ 5.4 eV) and has been used as a *p*-type dopant in carbon nanotubes¹ and graphene². We deposit ≈ 10 nm of F4TCNQ molecules on the Bi_2Se_3 Hall bar devices that are fabricated as described in the main text. Figure S1a shows Hall carrier density n_H at zero gate voltage and at room temperature for 15 devices with (red) or without (blue) F4TCNQ deposition ranging in thickness from 5 to 17 nm. On average, the deposition of F4TCNQ results in a change of doping of $-1 \times 10^{13} \text{cm}^{-2}$ (arrows in figure S1a); the negative sign indicates a shift toward *p*-type doping, i.e. a reduction in *n*-type doping.

Figure S1b shows conductivity $\sigma(n_H)$ of a F4TCNQ-doped 12 QL device at room temperature and ambient condition. The device were exposed to air for 1 (black square), 15 (red circle), and 25 (green triangle) days. The doping at zero gate voltage changes less than 10% in 15 days but shows negligible change from 15 to 25 days. We obtain the Hall mobility of ≈ 600 cm^2/Vs in all measurements, which shows good thermal stability of *p*-type doping by F4TCNQ molecules. This is in contrast to the behavior of Bi_2Se_3 device without F4TCNQ layer as surface degradation is commonly observed upon prolonged exposure to ambient^{3,4}. Therefore, we conclude that F4TCNQ not only provides effective *p*-type doping but also act as stable capping layer for protecting the Bi_2Se_3 surface from degradation.

2. Absence of activated insulating behavior in 5QL device.

Here we discuss the possible origin of metallic conduction in gapped TI thin films. Figure S2a shows resistivity ρ_{xx} of the 5 QL device as a function of gate voltage V_g and temperature T . The shift of maximum resistivity ρ_{max} (dashed line) is due to thermal activation from bulk valence band when the Fermi level E_f is close to charge neutrality point⁵. As can be seen in figure S2b, ρ_{xx} increases linearly with temperature for $T > 50\text{K}$, which is consistent with our previous study on electron-phonon scattering on the metallic TI surface⁵. The trace of $\rho_{\text{max}}(T)$ shows metallic behavior, i.e. $d\rho_{\text{max}}/dT > 0$ (inset of figure S2b). A weak insulating behavior ($d\rho_{\text{max}}/dT < 0$) can be seen for $T < 40$ K for data taken at fixed gate voltage (main panel figure S2b) but the temperature dependence is much weaker than thermal activation. Similar behavior was observed in MBE grown Bi_2Se_3 thin films and interpreted as electron-electron interaction corrections to the conductivity^{6,7}.

The hybridization induced energy gap Δ in few-QL Bi_2Se_3 has been measured in a recent ARPES study⁸. Transport experiment shows clearly insulating behavior in 3 QL thick Bi_2Se_3 field effect transistor, and energy gap as large as $\approx 250\text{meV}$ was estimated⁹. However, Δ is expected to decrease exponentially as a function of thickness. Moreover in the presence of finite disorder the surface, although gapped, can conduct through inhomogeneity-driven electron-hole puddles. For 5 QL device we estimate Δ from the fit to ARPES study⁸ to be $\approx 34\text{ meV}$. Previous scanning tunneling microscopy study of disorder driven electron-hole puddles in TIs¹⁰ shows energy fluctuation of about 10~16 meV for doped Bi_2Se_3 with amount of disorder $n_{\text{imp}} \approx 5 \times 10^{12}\text{cm}^{-2}$, which is comparable to $\Delta/2 \approx 17\text{ meV}$, and we generally estimate larger n_{imp} in micro-fabricated devices¹¹. This is a qualitative comparison only, since the screening will be poor for Fermi energies within the gap, and charge inhomogeneity will always create screening puddles with $E_F > \Delta/2$. However, the fact that the observed disorder scale for ungapped Bi_2Se_3 is comparable to the observed gap Δ is suggestive that our devices should be dominated by inhomogeneity. Therefore we conclude that the observed metallic temperature dependent resistivity in gapped TI thin films is due to conduction through inhomogeneity-driven electron-hole puddles.

References

1. Kazaoui, S., Guo, Y., Zhu, W., Kim, Y., & Minami, N. Optical absorption spectroscopy of single-wall carbon nanotubes doped with a TCNQ derivative *Synth. Met.* **135**, 753-754 (2003).
2. Coletti, C. *et al* Charge neutrality and band-gap tuning of epitaxial graphene on SiC by molecular doping. *Phys. Rev. B* **81**, 235401 (2010).
3. Kong, D. *et al*. Rapid Surface Oxidation as a Source of Surface Degradation Factor for Bi_2Se_3 . *ACS Nano* **5**, 4698-4703 (2011).

4. Analytis, J. G. et al. Two-dimensional surface state in the quantum limit of a topological insulator. *Nature Phys.* **6**, 960-964 (2010).
5. Kim, D. et al Intrinsic electron-phonon resistivity in Bi_2Se_3 in the topological regime *Phys. Rev. Lett.* **109**, 166801 (2012).
6. Wang, J. et al Evidence for electron-electron interaction in topological insulator thin films *Phys. Rev. B* **83**, 245438 (2011).
7. Liu, M. et al Electron interaction-driven insulating ground state in Bi_2Se_3 topological insulators in the two-dimensional limit *Phys. Rev. B* **83**, 165440 (2011).
8. Zhang, Y. et al. Crossover of the three-dimensional topological insulator Bi_2Se_3 to the two-dimensional limit *Nature Phys.* **6**, 584-588 (2010).
9. Cho, S., Butch, N. P., Paglione, J., & Fuhrer, M. S. Insulating behavior in ultrathin bismuth selenide field effect transistors. *Nano Lett.* **11**, 1925-1927 (2011).
10. Beidenkopf, H. et al. Spatial fluctuations of helical Dirac fermions on the surface of topological insulators. *Nature Phys.* **7**, 939-943 (2011)
11. Kim, D. et al. Surface conduction of topological Dirac electrons in bulk insulating Bi_2Se_3 *Nature Phys.* **8**, 460-464 (2012)

Figure S1.

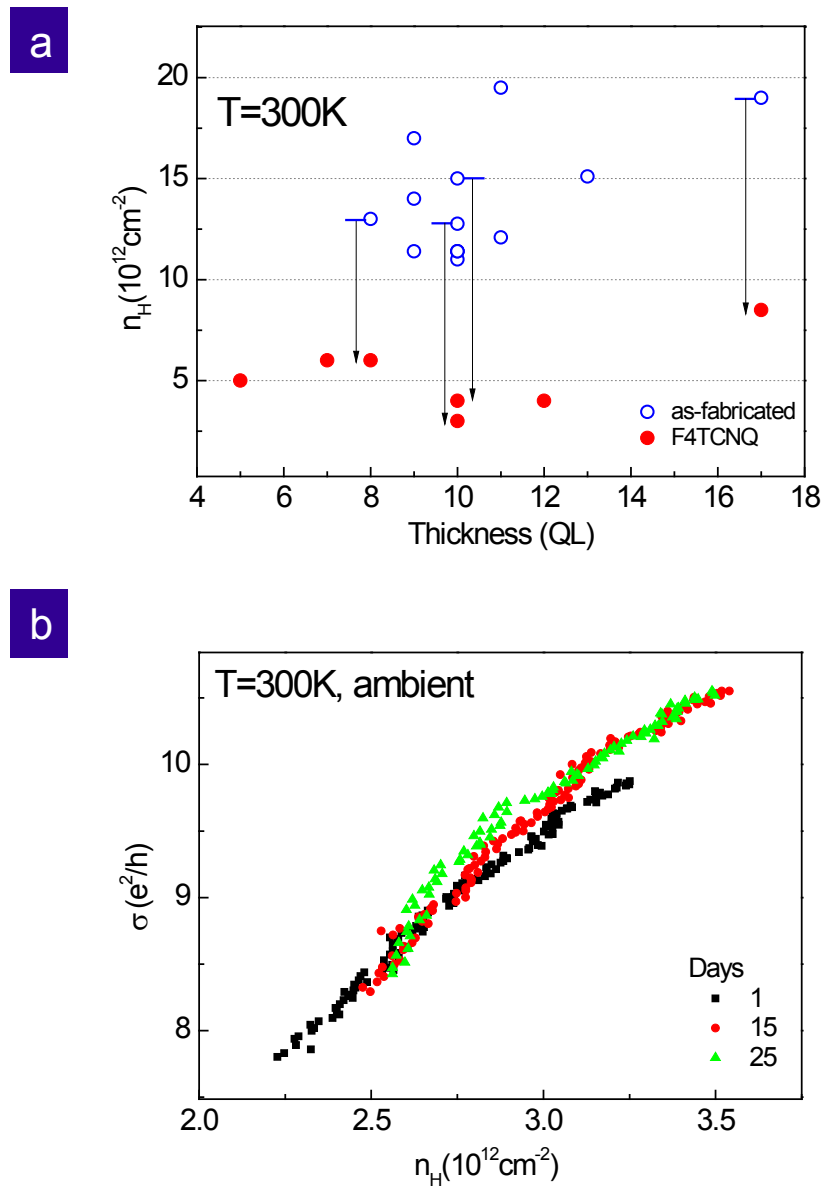


Figure S1 Charge transfer *p*-type doping with F4TCNQ. a, Hall carrier density n_H at zero gate voltage and at room temperature for 15 devices with (red) or without (blue) F4TCNQ deposition ranging in thickness from 5 to 17 nm. Arrows indicate change of n_H measured in the same sample. **b**, Conductivity σ of 12QL device as a function of n_H at 300 K and ambient condition. The device were exposed to air for 1 (black square), 15 (red circle), and 25 (green triangle) days. In all measurements the range of gate voltage is from 0 to -20 V.

Figure S2.

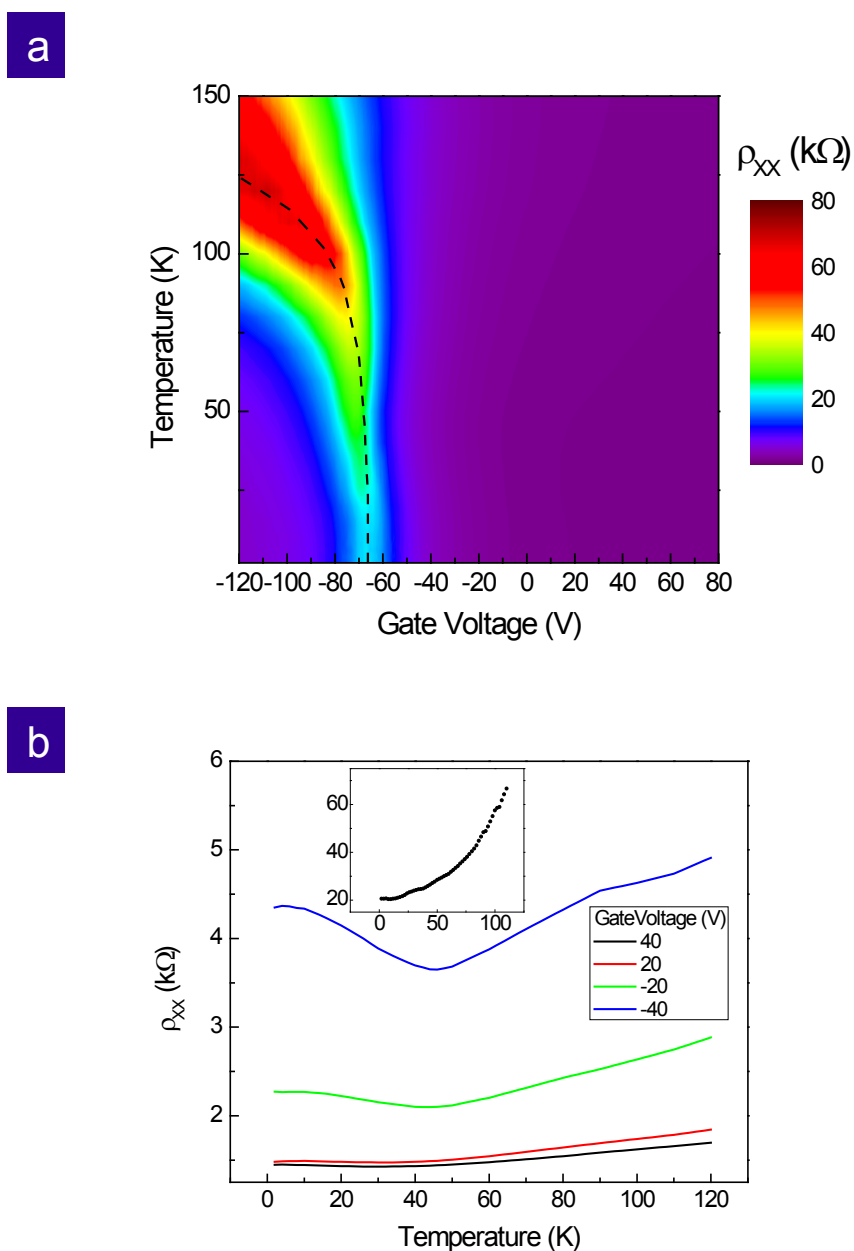


Figure S2 Temperature dependent resistivity in 5QL device. a, Longitudinal resistivity ρ_{xx} of the 5 QL device as a function of gate voltage V_g and temperature T . Dashed curve shows a trace of the position of ρ_{max} . **b,** ρ_{xx} vs. T at various gate voltages. The inset shows maximum resistivity ρ_{max} as a function of T .